Desalination and Water Treatment
www.deswater.com

doi:10.5004/dwt.2018.22735

124 (2018) 134–145
August

Cerium oxide nanoparticles anchored onto graphene oxide for the removal of heavy metal ions dissolved in water

Ada Rebeca Contreras Rodríguez[a], Joseph E. McCarthy[b], Amanda Alonso[a], J. Moral-Vico[a], Xavier Font[a], Yurii K. Guńko[b,c], Antoni Sánchez[a,*]

[a]*Department of Chemical, Biological and Environmental Engineering, Escola d'Enginyeria, Universitat Autònoma de Barcelona, 08193 Bellaterra, Spain, email: adarebecac@gmail.com (A.R.C. Rodríguez), Tel. +34935811018, email: Amanda.alonso@uab.cat (A. Alonso), Tel. +34935812789, email: antoniojavier.moral@uab.cat (J. Moral-Vico), Tel. +34935814480, email: Xavier.font@uab.cat (X. Font), Tel. +34-935814793, Fax +34-935812013, email: Antoni.sanchez@uab.cat (A. Sánchez)*
[b]*School of Chemistry, Trinity College Dublin, Dublin 2, Ireland, Tel. +35386088682, email: mccartj5@tcd.ie (J.E. McCarthy), Tel. +35318963543, email: igounko@tcd.ie (Y.K. Guńko)*
[c]*ITMO University, 197101 Saint Petersburg, Russia*

Received 24 October 2017; Accepted 1 July 2018

ABSTRACT

The aim of this study is to investigate the possibility of using cerium oxide (CeO_2) nanoparticles (NPs) attached to reduced graphene oxide (rGO) as an alternative adsorbent for cadmium (II), lead (II) and chromium (VI) removal from aqueous solution. The new nanomaterials (CeO_2/rGO) were obtained following two different strategies, in-situ growth and self-assembly approach. The adsorption capacities for each heavy metal were investigated at a fixed pH (5.5–6), a range concentration of heavy metal from 5 to 250 mg/L and a fixed concentration of 0.05 mg of CeO_2/rGO nanomaterial. The experimental data were fitted using the Langmuir, Freundlich and Temkin isotherms models. The experimental data of each nanomaterial for the removal of Pb(II) were approximated best by the Langmuir model, while for the removal of Cd(II) Langmuir and Freundlich showed good regression coefficients. The study showed that CeO_2 NPs attached to rGO could be used as an efficient adsorbent material for the adsorption of cadmium and lead from aqueous solution. The nanomaterial obtained by *in-situ* growth registered the highest adsorption capacity for the removal of lead (95.75 mg Pb^{2+}/g CeO_2/rGO-HMT), while in the case of cadmium the highest adsorption was obtained with the nanomaterial synthesized following the self-assembly approach (31.26 mg Cd^{2+}/g CeO_2/rGO-AM).

Keywords: Cerium oxide nanoparticles; In-situ growth; Self-assembly; Graphene oxide; Heavy metals removal; Nanocomposite

1. Introduction

Adsorption has been widely used for the removal of different types of pollutants in water, such as heavy metals and organic pollutants. There is a wide variety of adsorbents, usually composite materials, which can mix the properties of two inorganic materials or an inorganic material and a biomaterial for a better removal efficiency [1–3]. In this work the adsorption capacity of graphene and graphene oxide (GO)-Cerium oxide (CeO_2) nanocomposites for some heavy metals is studied.

Cerium oxide (CeO_2) is a rare earth oxide with a wide range of applications in catalysis, UV-blocking and oxygen sensors [4]. In addition, some studies used CeO_2 nanoparticles (NPs) as suitable adsorbents for the elimination of heavy metal ions [5–7]. Graphene and graphene oxide (GO) have been the hotspot in multidisciplinary areas due to their

*Corresponding author.

excellent mechanical, thermal, and electrical properties. In addition, both graphene and GO can be doped with metal oxides resulting in nanomaterials that usually have features that make them suitable materials for the effective sequestration of heavy metal ions due to their excellent adsorption performance [8,9]. Moreover, in the case of organic pollutants or persistent organic pollutants, those nanomaterials decompose the pollutants to less toxic molecules [10].

One of the biggest limiting steps in the application of graphene-based nanomaterials in environmental fields is the agglomeration of the graphene sheets to form graphite due to Van der Waals interactions. To overcome this drawback, a growing exploration to modify (due to the presence of oxygen containing functional groups on their surface), immobilize or anchor NPs or other materials onto graphene has been tested [11]. Different approaches have been studied for the synthesis of hybrid nanomaterials based on graphene and metal NPs [12–14]. Recent studies suggest that reduced graphene oxide (rGO) and GO supported materials have higher binding capacity compared to free NPs [15]. Additionally, another aspect to take into account for using such composites for application in environmental remediation, such as water purification, is the ease of solid–liquid separation and post treatment handling [15–17].

In this study, two different strategies to obtain a hybrid material composed of CeO_2 NPs anchored to the surface of GO: *self-assembly* approach and *in-situ* growth, followed by a chemical reduction of the GO becoming CeO_2/rGO, in both cases. The *self-assembly* approach is based in a two-step synthesis, in which the first step is to synthesize the NPs with specific dimensions and morphologies using different stabilizers, such as 6-aminohexanoic acid (AHA) [1] or hexamethylenetetramine (HMT) [18], followed by the attachment of the NPs on the surface of the GO in a second step. On the other hand, the *in-situ* growth suggests the growth of NPs directly in the basal planes of the graphene oxide [4]. In most hybrid materials, the metal NPs deposited on graphene often exhibit agglomeration under the high temperature used in the synthesis. Many studies suggest the addition of organic additives such as acrylamide (AM) [19] or poly(vinylpyrrolidone) (PVP) [4] to control the NPs dispersion and size.

In this work, the *in-situ* strategy is based on the electrostatic adsorption of positively charged Ce^{3+} ions on the basal planes of GO sheets, that are highly negatively charged when dispersed in water [20], followed by in situ growth of CeO_2 on GO sheets, and finally the conversion of GO into rGO. On the other hand, the *self-assembly* strategies go through the direct deposition of CeO_2 NPs on the surface of the GO sheets followed by the reduction of GO to rGO [4,20].

According to Ji et al. [4], during the *self-assembly* process of the CeO_2/rGO-AHA nanomaterial, the AHA-stabilized CeO_2 was prepared as a first step, in which the carboxylic acid of the AHA binds to the surface of the CeO_2 NPs and releases a proton to form a carboxylate group. The proton then protonates the amino group of AHA, generating a positively charged surface for the CeO_2 NPs [21]. As mentioned before, the assembly of the CeO_2 NPs (stabilized with AHA) on the GO sheets is provided by the electrostatic interactions between the surface of the NPs and the surface of the GO, creating a well combined nanocomposite [4].

The objective of this study was to investigate the influence of these two strategies in the distribution and size of the NPs and thus, in their properties as adsorbents. Furthermore, the adsorption capacity for cadmium (II), lead (II) and chromium (VI) ions onto the new nanomaterials synthetized was tested and fitted using Langmuir, Freundlich and Temkin isotherm adsorption models. To the best of our knowledge, this is the first study where GO derived materials are effectively used for the removal of highly toxic heavy metals in a wide range of concentrations. Another important objective to highlight is to determine how the difference in the synthesis of these advanced adsorbent nanomaterials can condition their further behavior.

2. Experimental

2.1. Synthetic protocols

2.1.1. Synthesis of GO and assembly of CeO_2 NPs onto GO sheets

GO was prepared from bulk graphite (Alfa Aesar) via the Hummers method [19]. Once the GO is synthesized the strategies of *self-assembly* and *in-situ growth* are used as routes to obtain a hybrid nanomaterial constituted of CeO_2 NPs onrGO, obtaining then, the CeO_2/rGO nanomaterial.

2.1.2. Synthesis of 6-aminohexanoic acid CeO_2 NPs and their deposition onto GO by self-assembly approach.

The method to synthesize AHA-stabilized CeO_2 NPs can be found in the literature using some modifications [4]. Firstly, a solution containing 0.87 g of $Ce(NO_3)_3{\cdot}6H_2O$ and 80 ml of deionized water was heated up to 95°C under magnetic stirring. Then, 8 ml aqueous solution with 1.05 g of AHA and 40 µl of 37% HCl solution were added in sequence to the previous solution. The final solution was kept at 95°C for 6 h. The resultant solution is a homogeneous suspension containing positively charged CeO_2 NPs.

Subsequently, the assembly process was conducted by mixing the CeO_2-AHA NPs and GO nanosheets, followed by a reduction process of the GO to rGO. To obtain the negatively charged GO nanosheets a colloidal dispersion of 130 mg of graphite oxide and 433.33 mg of PVP were dispersed in 345 ml of deionized water by sonication for about 30 min. Afterwards 43.33 ml of positively charged CeO_2-AHA suspension was slowly added under magnetic stirring. After 4 h of stirring, 2 ml (2 mM) of ascorbic acid were added to the above solution. The resulting mixture was refluxed at 95°C for 1 h. The solid product was separated by centrifugation and well washed with water and ethanol to remove any impurities and then dried at 50°C for 24 h. Finally, the obtained product was designed as CeO_2/rGO-AHA.

2.1.3. Synthesis of acrylamide CeO_2 NPs and their deposition onto GO by self-assembly approach

The method followed to synthesize the CeO_2/rGO-AM was previously describe by Ling et al. [20]. A solution of 1 mM $Ce(NO)_3{\cdot}6H_2O$ and 5 mM AM were dissolved in 26 ml

of N,N-dimethylformamide (DMF) with ultrasonic treatment. At the same time, 130 mg of GO were dispersed into 260 ml distilled water also with ultrasonic treatment for 2 h to form a brown solution.

For the assembly, the above two solutions were mixed and heated at 90°C with continuous stirring for 1 h. Then, 2 ml of ascorbic acid (2 mM) were added to reduce the GO and the solutions were refluxed at 90°C for 6 h. The solid was separated by centrifugation and washed several times with ethanol and distilled water before drying at 60°C for 24 h. The final product is designed as CeO_2/rGO-AM.

2.1.4. Synthesis of CeO_2 NPs with hexamethylenetetramine and their deposition onto GO by in-situ growth

The synthesis of CeO_2 NPs by using HMT was performed with an *in-situ* growth. The synthetic procedure followed the conditions to precipitate the CeO_2 NPs reported by Zhang et al. [15] with the following modifications in order to achieve stabilization. A solution of 0.5 mM AM dissolved in 20 ml DMF with ultrasonic treatment is mixed with 0.04 M of $Ce(NO_3)_3{\cdot}6H_2O$ under stirring for 30 min. Then, a solution of HMT 0.5 M and 130 mg of GO, also with ultrasonic treatment, was added to the previous solution. After 1 h stirring 2 ml of 2 mM of ascorbic acid was added. The final solution was maintained under mild stirring and room temperature for 24 h. The product was washed several times with ethanol and water and dried at 60°C for 24 h. The nanocomposite material is designed as CeO_2/rGO-HMT.

2.2. Characterization methods

2.2.1. Raman spectrometry

Raman spectra were recorded using a Renishaw 1000 micro-Raman system fitted with a Leica microscope and the Grams Research™ analysis software. The excitation wavelength was 633 nm from a Renishaw RL633 HeNe laser. The 50× magnifying objective of the Leica microscope was capable of focusing the beam onto a spot of approximately 2–3 μm in diameter. Analysis was performed at the Trinity College (Dublin).

2.2.2. Transmission electron microscopy (TEM)

TEM images were obtained on a JEOL JEM-2100. Samples were prepared by deposition of each of the CeO_2/rGO nanomaterials dispersed in water onto a carbon coated 300 mesh copper grid. Diameters were measured with the Image J software program and the average values were calculated by counting a minimum of 100 particles. Analysis performed in the CRANN Advanced Microscopy Facility (AML) at Trinity College (Dublin).

2.2.3. Metal determination by inductively coupled plasma-optical emission spectrometry

The samples solutions containing heavy metal ions were acidified with concentrated HNO_3 (Merck, p.a. quality) until HNO_3 1% (p/v). The determination of the concentration of cadmium (II), lead (II) and chromium (VI) was performed by Inductively Coupled Plasma-Optical Emission Spectrometry, ICP-OES, Perkin-Elmer Optima 4300DV model. The experimental analysis was performed by the *Serveid'Anàlisi Química* at the Autonomous University of Barcelona.

2.3. Metal adsorption experiments and isotherm models

The adsorption experiments were performed using cadmium (II) chloride (99.9%), lead (II) nitrate (99.9%) and potassium dichromate (VI) (99.5%) as metal sources. To test the adsorption capacity and determine the adsorption isotherms of the different nanomaterials synthesized in a wide range of metal concentration, eight dilutions of cadmium, lead and chromium (5, 30 50, 100, 150, 200, and 250 mg/L) were carried out. Each of these solutions were mixed with 0.05 mg of CeO_2/rGO (HMT, AM and AHA) nanomaterial. rGO was used as control at the same conditions. All the experiments were stirred at 200 rpm at room temperature for 24 h. No adjustment in the pH was performed (pH = 5.5–6). The samples were filtrated (40 μm) to separate the nanomaterial (solid phase) from the liquid phase. The supernatant was analyzed for residual dissolved heavy metals (non-adsorbed metal). The adsorption capacity at the equilibrium was calculated with the following equation [23]:

$$q = (C_0 - C_e)V/m \quad (1)$$

where C_0 and C_e are the initial and equilibrium concentrations of the heavy metal (mg/L) respectively, V is the volume (L) and m (g) is the mass of the NPs.

Normally, the adsorption of metal ions from aqueous solutions is largely based on ion exchanges or chemical/physical adsorptions on specific sites of the adsorbents, and therefore the pore structures and surface areas of the adsorbents would play a crucial role [24]. Equilibrium adsorption isotherms are typically used to determine the capacities of adsorbents. The most common models used are the Langmuir, Temkin and the Freundlich models. Therefore, these models were used to fit the experimental data [23]. The linear forms of the Langmuir, Temkin and Freundlich models are listed in Table 1.

3. Results and discussion

3.1. Structural characterization of the nanomaterials

We have described two different strategies for the fabrication of CeO_2/rGO nanomaterials: *in situ* growth to obtain CeO_2/rGO-HMT and the *self-assembly* approach to obtain CeO_2/rGO-AHA and CeO_2/rGO-AM. The synthetic protocols for obtaining the nanocomposites are described in Fig. 1.

For the formation of CeO_2/RGO-AM nanomaterial, Ling et al. [19] proposed a similar *self-assembly* approach. Briefly, the AM is hydrolyzed to produce a polymer that reacts with the metal ions and forms a polymer metal complex (PMC), where the cerium ions and the amino groups are bonded. The PMC with a positive charge is

attracted by the GO negatively charged and the self-assembly befalls once again by electrostatic attraction; therefore the metal ions are anchored to the surface of the GO maintaining the layered structure and finally reduced with ascorbic acid.

In the case of the *in-situ synthesis* the methodology proposed by Zhang et al. [18] to obtain CeO_2 NPs was used with some modifications. In this work, the AM is added in the first step (hydrolysis of the cerium salt) of the synthesis of CeO_2 NPs using HMT to form the PMC, which generates a positive charge in the surface and favors the dispersion of the NPs on the surface of the GO, as shown in the above synthesis. The GO is directly mixed with the HMT and then added to the cerium solution so that the hydroxyl ions oxidize the cerium to obtain the NPs anchored on the surface of the GO [25]. Each product was characterized by Raman spectroscopy and transmission electron microscopy.

3.2. Raman spectroscopy

Raman scattering is a powerful tool to characterize carbon based materials in a non-destructive way. The most prominent features in the Raman spectra of monolayer graphene are the so-called G-band appearing at 1582 cm^{-1} (graphite) and the G-band at about 2700 cm^{-1}, using laser excitation at 2.41 eV. Fig. 2 shows the Raman spectra of the CeO_2/rGO-AHA (by self-assembly), CeO_2/rGO-HMT (by in-situ) and the rGO. Two distinct peaks corresponding to the well-known G and D bands are displayed. The G band is usually assigned to the vibration of sp^2 carbon atoms in a graphitic 2D hexagonal lattice, while the D band is associated with the vibrations of sp^3 carbon atoms of defects and disorder [4,8]. In a typical synthesis, rGO showed D-band at 1345 cm^{-1} and G-band at 1598 cm^{-1}. After the reduction, the D-band remained the same but G-band shifted to lower frequency region (1580 cm^{-1}), confirming the reduction [12]. The corresponding peak for CeO_2 NPs has been reported between 462 cm^{-1} and 467 cm^{-1} [19,26,27], however the peak at 455 cm^{-1} present in Fig. 1 is attributed to CeO_2 NPs, and the shift associated to the successful attachment on the rGO in both CeO_2 composites. Furthermore, a difference in the signal intensity for the peaks corresponding to both the CeO_2 NPs and rGO is observed, obtaining a NPs/rGO intensity ratio higher for the CeO_2/rGO-HMT (Fig. 2b) than for CeO_2/rGO-AHA (Fig. 2c). This result could suggest a higher concentration of CeO_2NPs for the in-situ mechanism of the CeO_2/rGO-HMT nanocomposite.

Table 1
Summary of equilibrium isotherms (K_L, K_F, K_T: Langmuir, Freundlich, Temkin constants; n: heterogeneity coefficient; q_m: maximum adsorption capacity; q_e: adsorption capacity at equilibrium; C_e: equilibrium concentration; b: activity coefficient related to mean sorption energy)

Isotherm model	Equation
Langmuir	$C_e/q_e = 1/K_L q_m + C_e/q_m$
Freundlich	$\log q_e = \log K_F + 1/n \log C_e$
Temkin	$q_e = Rt/b \ln K_T + RT/b \ln C_e$

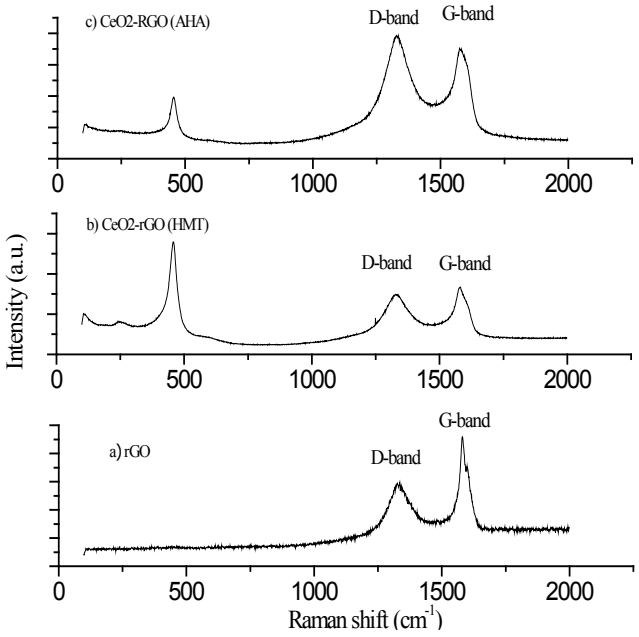

Fig. 2. Raman spectra of (a) rGO, (b) CeO_2/rGO-HMT by *in situ* and (c) CeO_2/rGO-AHA by *self-assembly.*

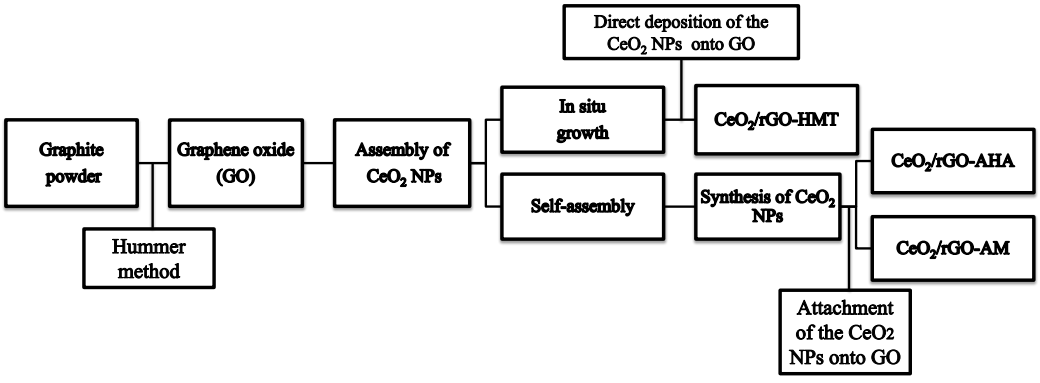

Fig. 1. Synthesis of CeO_2/rGO nanocomposites by in situ growth and self-assembly method.

3.3. Transmission electron microscopy (TEM)

TEM technique was used to elucidate the size, morphology and microstructure of the rGO-based nanomaterials, by dropping a small quantity of the dispersion onto holey carbon grids [28]. Fig. 3 shows the TEM images of the CeO_2/rGO nanomaterials prepared by both strategies: *self-assembly*, CeO_2/rGO-AM and CeO_2/rGO-AHA and, *in situ* growth, CeO_2/rGO-HMT, as well as their size distribution.

As shown in Fig. 3A, CeO_2/rGO-AM is uniformly deposited and dispersed on the reduced graphene oxide. The size distribution of the CeO_2 –AM NPs falls in the range of 2.10±0.40 nm (Fig. 2A'). Fig. 3B shows CeO_2-AHA NPs deposited on the surface of the rGO with a distribution size of 16.12±2.24 nm (Fig. 3B'). Although the *self-assembly* approach involves two steps in order to obtain the nanocomposite, this feature allows a good control of the NPs size. The TEM image of the CeO_2/rGO-HMT (Fig. 3C) presents high density of CeO_2-NPs attached to the rGO with a NPs distribution size in the range of 3.343±0.701 nm (Fig. 2C'). The distribution size parameters are detailed in *Supplementary Information, S.I.2*. The higher concentration of the NPs, observed here, was also demonstrated with the previously discussed Raman results. The *in situ* synthesis possesses the advantage of fabricating the nanomaterial in one step. However, the morphology and the distribution of the nanoparticles cannot be well controlled due to many

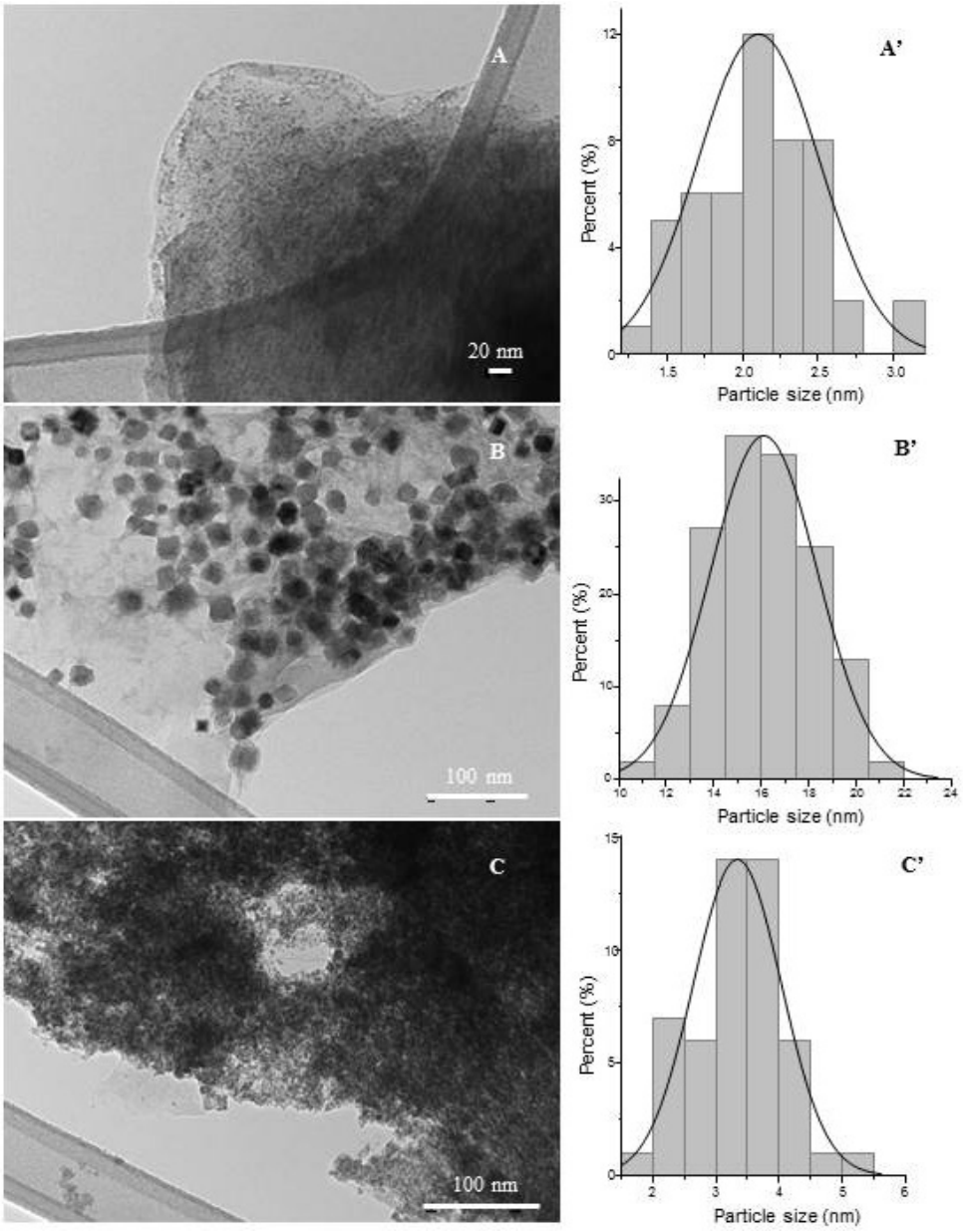

Fig. 3. TEM images of (A) CeO_2/rGO-AM, (B) CeO_2/rGO-AHA and (C) CeO_2/rGO-HMT nanocomposites as well as the size distribution (A', B' and C').

factors, such as defects in the surface of the GO sheet, temperature, etc. [16].

3.4. Adsorption isotherms

The adsorption of lead (II), cadmium (II) and chromium (VI) from aqueous solutions onto rGO nanosheets impregnated with CeO_2-NPs synthetized by the different mentioned protocols were tested.

Respectively, Tables 2 and 3 show the adsorption capacities of lead (II) and cadmium (II) with each adsorbent here reported, as well as the final metal concentration. It was observed that mainly lead (II) showed changes in the concentration (Table 2), while cadmium (II) was adsorbed at lower concentrations (Table 3). The adsorption of chromium (VI) in solution does not follow a clear tendency and no adsorption model could be applied. A possible reason for this behavior is that although chromium is dissolved as hexavalent chromium, chromium is actually present in its anionic form, thus the repulsion with the negative charge of the rGO appears to be stronger than the interaction with the NPs, showing very little affinity for the nanomaterial.

The highest adsorption capacity was obtained for the CeO_2/rGO-HMT material (95.75 mg Pb^{2+}/g CeO_2/rGO-HMT), almost double than that obtained with the rGO (49.927 mg Pb^{2+}/g rGO), and significantly higher than the other self-assembly synthetized nanomaterials (46.78 mg Pb^{2+}/g CeO_2/rGO-AHA and 62.80 mg Pb^{2+}/g CeO_2/rGO-AM). The obtained adsorption capacity is in the middle range of reported literature values. While non-nanomaterials such as *Ficusreligiosa* leaves showed lower adsorption capacities (37.45 mg Pb^{2+}/g) [29], plant maize (2.3 mg Pb^{2+}/g) [30] or bagasse fly ash, (2.50 mg Pb^{2+}/g) [31]; some metal oxide NPs (181.2 mg Pb^{2+}/g CeO_2 and 153.24 mg Pb^{2+}/g TiO_2) [6] showed higher adsorption capacities than the rGO-based nanocomposites here presented.

From the adsorption capacity values for the removal of cadmium (Table 3), it can be observed that the maximum value was obtained with the CeO_2/rGO-AM, being 31.26 mg Cd^{2+}/ g CeO_2/rGO-AM, which is double than the one corresponding to rGO (15.42 mg Cd^{2+}/g rGO). It can be seen that the values obtained with GO are similar to the ones obtained with CeO_2/rGO-HMT (11.67 mg Cd^{2+}/g CeO_2/rGO-HMT) and CeO_2/rGO-AHA (16.71 mg Cd^{2+}/g CeO_2/rGO-AHA), which can be compared

Table 2
Adsorption experiments for the removal of Pb (II) dissolved in water with different CeO_2/rGO nanomaterials. C_e is the concentration of the metal ions at equilibrium; q_t is the adsorption capacity measured after 24 h and expressed in mg metal/g nanomaterial; *Higher than the initial concentration; N/A: not available

Initial	Adsorption capacities, removal percentages and final metal concentrations											
Pb (II) concentration	rGO			CeO_2/rGO-AHA			CeO_2/rGO-AM			CeO_2/rGO-HMT		
Ci (mg/L)	C_e (mg/L)	q_t (mg/g)	%Removal	C_e (mg/L)	q_t (mg/g)	%Removal	C_e (mg/L)	q_t (mg/g)	%Removal	C_e (mg/L)	q_t (mg/g)	%Removal
5	0.5	18	90	0.73	17.1	85.49	0.59	17.62	88.1	0.5	18	90
10	2.04	31.85	79.63	2.95	28.21	70.52	3.99	24.02	60.06	2.37	30.53	76.33
30	22.56	29.77	24.81	19.84	40.65	33.88	22.5	29.98	24.99	16.29	54.85	45.71
50	40.85	36.58	18.29	38.04	47.85	23.93	42.78	28.89	14.44	30.95	76.19	38.09
100	87.52	49.93	12.48	85.55	57.8	14.45	91.43	34.28	8.57	77.54	89.84	22.46
150	*	N/A	N/A	137.92	48.32	8.05	141.55	33.79	5.63	132.56	69.77	11.63
200	196.02	15.9	1.99	187.08	51.7	6.46	186.36	54.54	6.82	182.86	68.56	8.57
250	*	N/A	N/A	238.3	46.78	4.68	234.3	62.8	6.28	226.06	95.76	9.58

Table 3
Adsorption experiments for the removal of Cd (II) dissolved in water with different CeO_2/rGO nanomaterials. *Higher than the initial concentration; C_e: concentration of the metal ions at equilibrium; q_t: adsorption capacity measured after 24 h and expressed in mg metal/g nanomaterial; N/A: not available

Initial	Adsorption capacities, removal percentages and final metal concentrations											
Cd(II) concentration	rGO			CeO_2/rGO-AHA			CeO_2/rGO-AM			CeO_2/rGO-HMT		
C_i (mg/L)	C_e (mg/L)	q_t (mg/g)	%Removal	C_e (mg/L)	q_t (mg/g)	%Removal	C_e (mg/L)	q_t (mg/g)	%Removal	C_e (mg/L)	q_t (mg/g)	%Removal
5	2.47	10.11	50.56	4.49	2.03	10.13	2.82	8.71	43.57	3.32	6.72	33.6
10	6.14	15.43	38.57	9.2	3.19	7.98	7.77	8.92	22.3	7.08	11.67	29.19
30	27.24	11.03	9.19	30.58	N/A	-1.93	28.85	4.58	3.82	27.1	11.57	9.64
50	49	4	2	45.82	16.71	8.36	49.08	3.69	1.84	50.01	N/A	N/A
100	*	N/A	N/A	*	N/A	N/A	99.47	2.12	0.53	*	N/A	N/A
150	*	N/A	N/A	*	N/A	N/A	*	N/A	N/A	*	N/A	N/A
200	*	N/A	N/A	*	N/A	N/A	196.73	13.08	1.64	*	N/A	N/A
250	*	N/A	N/A	*	N/A	N/A	242.18	31.26	3.13	*	N/A	N/A

with those obtained with Filtrasorb 400 (9.5 mg Cd^{2+}/g) [32], carbon aerogel (15.5 Cd^{2+}/g) [33], Indonesian peat (14 mg Cd^{2+}/g) [34] or TiO_2 (15.83 mg Cd^{2+}/g TiO_2) [5], while Fe_3O_4 (99.57 mg Cd^{2+}/g Fe_3O_4) [5] and CeO_2 (48.30 mg Cd^{2+}/g CeO_2) [5] presented higher adsorption capacities. Even though CeO_2 NPs by themselves showed higher adsorption capacity for Cd^{2+} than the materials here reported, it is worth saying that the CeO_2 based nanosheets present other advantages including NPs stability. Pb(II) ions showed higher removal percentages than Cd(II) ions, which is in agreement with the metal electronegativity associated to each metal.

Electronegativity can be treated as one of the important parameters in the metal cation uptake of the adsorption process, since a negatively charged surface plays an important role, and the electronegativity of Pb^{2+} is higher than Cd^{2+} [35].

These results can be attributed not only to the high surface area due to the presence of the CeO_2 NPs and its composition, but also to the high oxygen content of GO [17]. In addition, the abundant oxygenated functional groups on the surfaces of GO nanosheets make the adjacent oxygen atoms available to bind metal ions [36].

The optimization of an adsorption process requires an understanding of the driving forces that govern the interaction between adsorbate and adsorbent, therefore it is important to establish the most appropriate correlation for the equilibrium [1,2]. The data obtained for the removal of cadmium (II) and lead (II) in adsorption were fitted to the Freundlich, Langmuir and Temkin isotherm models. The sorption behavior for each metal ion onto the different nanomaterials is shown in Fig. 4. The parameters of each adsorption model were calculated and listed in the Table 4. Only the available data obtained from the adsorption experiments was used in the fitting of the adsorption models. The regression coefficient (R^2) shows that the Langmuir model fitted better than the Freundlich and the Temkin models in the case of Pb(II), suggesting that Pb(II) ions adsorption on the three different nanocomposites and therGO are all monolayer coverage. The Langmuir isotherm is the best one describing the chemisorption processes. Chemisorption involves a more specific binding of the adsorbate to the solid, in this case of the heavy metal ion to the CeO_2/rGO nanocomposite. It is a process that is more similar to a chemical reaction, involving valence forces through sharing or exchanging electrons between sorbent and sorbate and hence, making only monolayer adsorption possible (i.e. oxygen atoms binding with metal ions) [37]. Sitko et al. [35] investigated the XPS spectra for GO with adsorbed divalent metal ions, among them Cd(II) and Pb(II), and observed a significant difference between oxygen peaks, suggesting that the nature of the adsorption of the metal ions on GO is chemical, in accordance with the process described by the Langmuir model. In addition, the point of zero charge (pHpzc) value of GO is 3.8–3.9. Therefore, at pH > 3.9, the surface charge of GO is negative and the electrostatic interactions between the metal ions and GO nanosheets become stronger [36,38–40]. On the other hand Cao et al. [41] synthesized ceria hollow nanospheres composed of CeO_2 nanocrystals and used them as adsorbent for the removal of As(V), Cr(VI) and Pb(II). They suggest that the adsorption mechanisms of the heavy metals ions on the metal oxide are likely the combination of static electrical attraction between oxides and heavy metal ions and metal ion exchange.

The Temkin isotherm contains a factor (b) that explicitly takes into account adsorbent–adsorbate interactions. By ignoring the extremely low and large value of concentrations, the model assumes that heat of adsorption (which is function of temperature) of all molecules in the layer would decrease linearly rather than logarithmic with coverage [42,43]. On the other hand, the Freundlich coefficient (n), which should have values ranging from 1 to 10 and in this case is high (5.28–6.76), supporting the favorable adsorption of the lead ions onto the adsorbent [44].

In Table 4 it is possible to observe that the data obtained for the removal of cadmium (II). In the case ofrGO the adsorption did not fit the linear models (negative coefficients), leading to the conclusion that the adsorption behavior of the tested systems was very difficult. However, the Langmuir isotherm fits quite well the adsorption data of CeO_2 composites, except for the case of CeO_2/rGO-AHA, which is well fitted by Freundlich and Temkin isotherms.

Overall, the *self-assembly* approach produced nanomaterials with CeO_2 NPs with controlled size on rGO sheets. This is a key step in the process for the preparation of well-defined NPs to position itself as an advantageous synthetic procedure [4]. However, the material synthesized by *in-situ* growth simplifies the process avoiding a prior step in the preparation of the CeO_2 NPs.

The adsorption results suggest that the new CeO_2-rGO nanocomposites synthesized by two different procedures presented promising results for adsorption of cationic water contaminants. The adsorption mechanism has contribution from both the negative functional groups of the rGO and the surface of the CeO_2-NPs.

Moreover, these reported methods offer potentially low cost and large scale production of graphene-based hybrid materials suitable for water purification [45]. This is due to the fact that the inorganic nanoparticles present in 2D graphene nanocomposites prevent graphene aggregation, and hence a high surface area and pore volume can be maintained [17].

4. Conclusions

Graphene oxide and CeO_2/rGO nanocomposites were successfully synthesized. Raman spectroscopy showed the peak associated to the G (1580 cm^{-1}) and D (1345 cm^{-1}) bands of the rGO and the peak of the CeO_2 NPs at 455 cm^{-1}, which confirms that cerium oxide nanoparticles were anchored to the surface. The size of the CeO_2 NPs attached to GO, ranged from 2 nm to 16 nm (depending on the synthesis pathway). The highest percentage removal (90%) was obtained with CeO_2/rGO-HMT nanocomposite for the case of Pb(II). The R^2 for Langmuir (0.907–0.994) isotherm model suggests chemisorption and monolayer coverage. Although Pb(II) and Cd(II) showed the main adsorption capacities, Cr(VI) was removed at lower concentrations. Future studies will explore the recycling of the nanomaterial to give a better understanding of the reusability of the adsorbent. Another important parameter will be to test the nanomate-

rial in multicomponent systems as a first step towards their use with real wastewaters.

Supporting Information. Size distribution parameters as Supporting Information is included.

Acknowledgments

A.R. Contreras Rodríguez thanks the financial support through the scholarship provided by the Consejo Nacional de Ciencia y Tecnología (CONACYT, México).

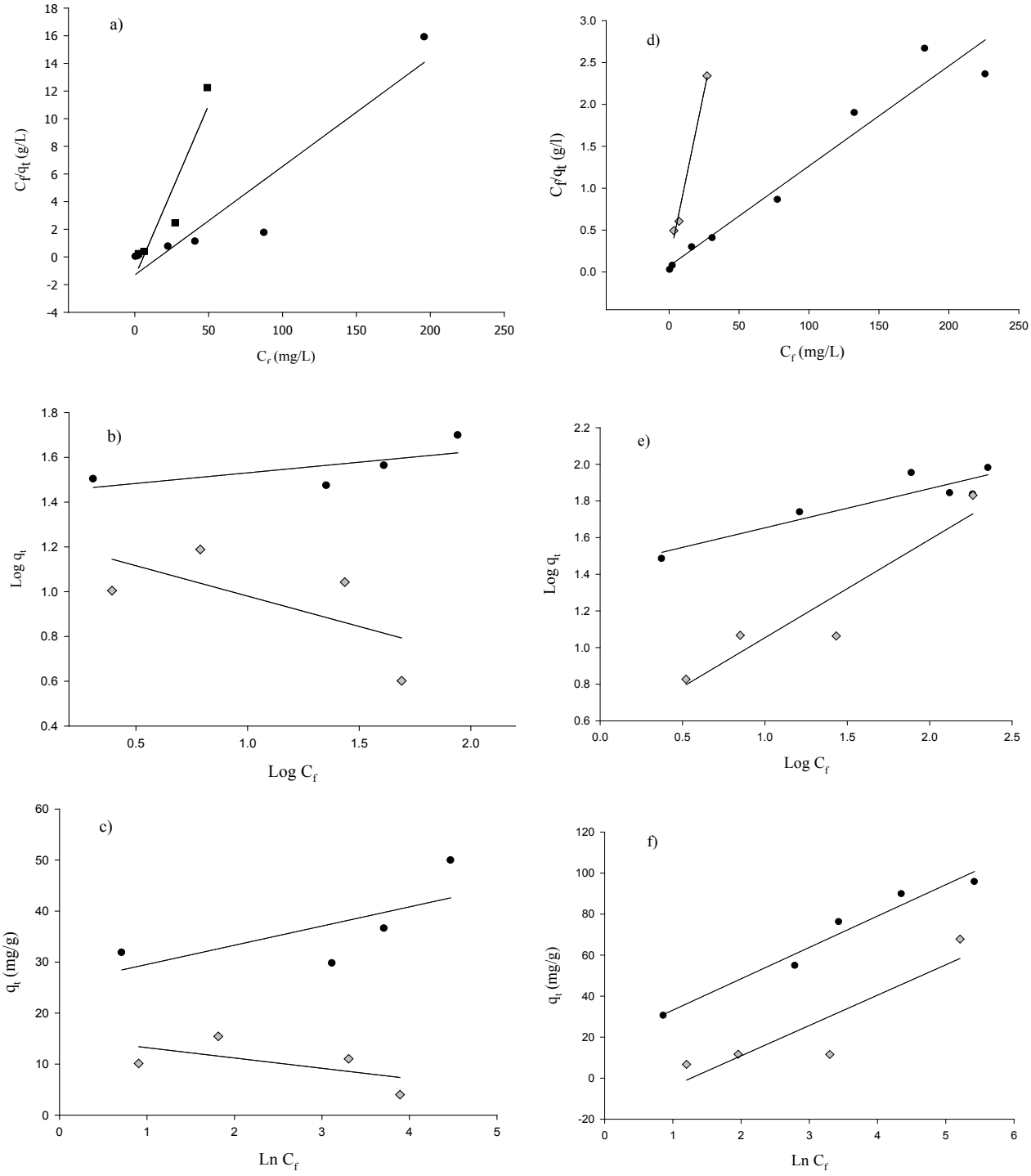

Fig. 4. a) Langmuir isotherm , b) Freundlich isotherm, c) Temkin isotherm for the adsorption of Pb(II) (dark circle) and Cd (II) (grey diamond) onto rGO; d) Langmuir isotherm, e) Freundlich isotherm, f) Temkin isotherm for the adsorption of Pb(II) (dark circle) and Cd (II) (grey diamond) onto CeO_2/rGO-HTM. (*Continued*)

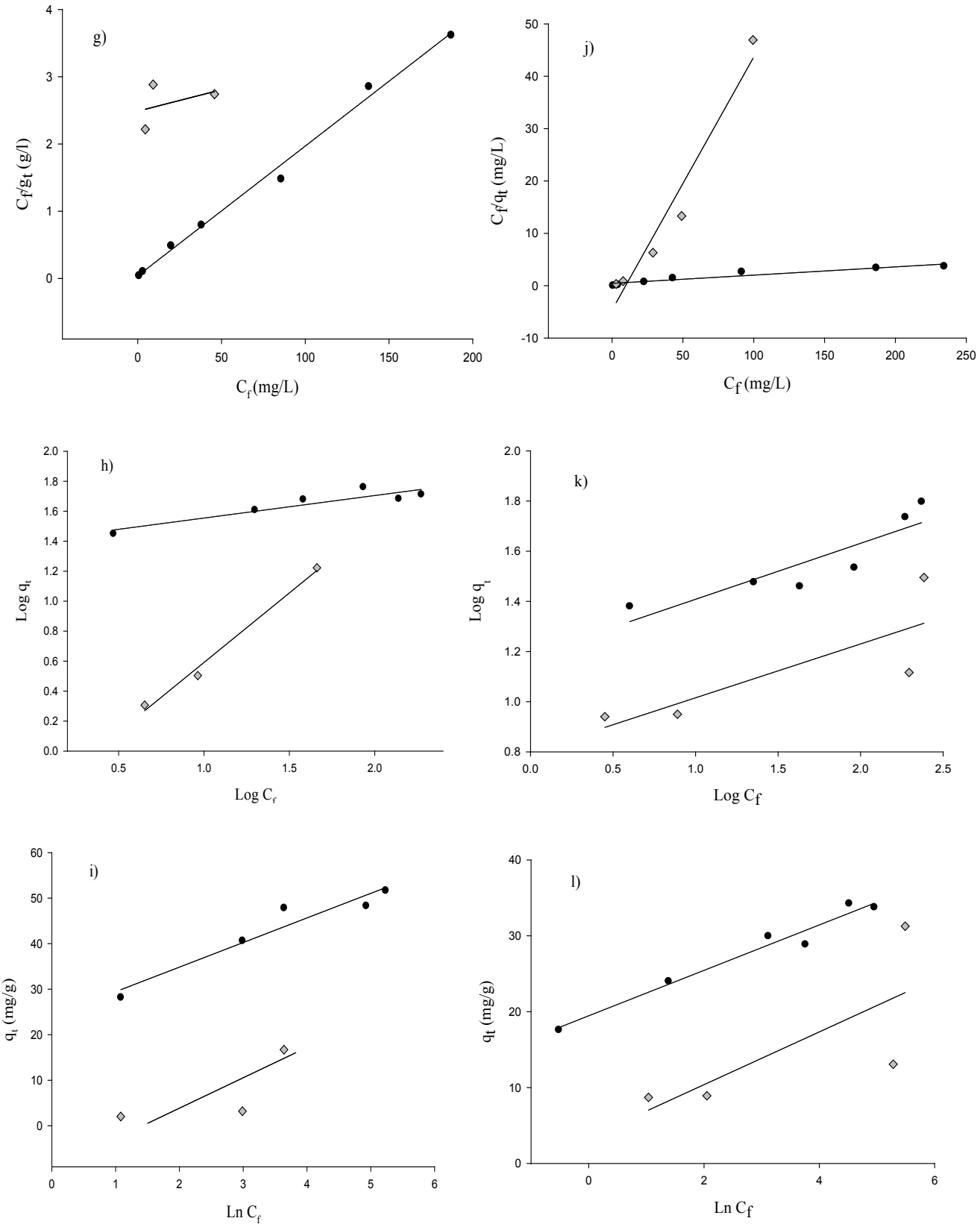

Fig. 4. (*Continued*) g) Langmuir isotherm , h) Freundlich isotherm, i) Temkin isotherm for the adsorption of Pb(II) (dark circle) and Cd (II) (grey diamond) onto CeO_2/rGO-AHA; j) Langmuir isotherm, k) Freundlich isotherm, l) Temkin isotherm for the adsorption of Pb(II) (circle) and Cd (II) (diamond) onto CeO_2/rGO-AM.

Table 4
Parameters for Langmuir, Freundlich and Temkin models of Pb(II) and Cd(II) ions adsorption on different CeO_2/rGO nanomaterials and rGO as reference sample

Isotherm	Adsorbent	Lead			Cadmium		
		Parameter			Parameter		
		q_m (mg/g)	K_L (L/mg)	R^2	q_m (mg/g)	K_L (L/mg)	R^2
Langmuir	rGO	50.25	0.15	0.9066	4.024	–0.17	0.8797
	CeO_2/rGO-HMT	83.33	0.07	0.9477	12.39	0.58	0.9913
	CeO_2/rGO-AHA	48.78	0.52	0.9937	156.25	0.003	0.1694
	CeO_2/rGO-AM	63.69	0.04	0.9145	14.12	0.05	0.9212
		K_F	n	R^2	K_F	n	R^2
Freundlich	rGO	22.46	6.68	0.7673	17.85	–3.68	0.4111
	CeO_2/rGO-HMT	23.86	4.05	0.9238	3.29	1.86	0.879
	CeO_2/rGO-AHA	20.89	5.05	0.9119	0.46	1.08	0.9900
	CeO_2/rGO-AM	17.77	5.28	0.8538	6.33	4.64	0.6627
		K_T	b	R^2	K_T	B	R^2
Temkin	rGO	126.97	4.56	0.7314	0.001	–2.04	0.6481
	CeO_2/rGO-HMT	5.44	13.87	0.9674	0.28	14.80	0.8043
	CeO_2/rGO-AHA	31.50	6.11	0.9603	0.24	6.68	0.9459
	CeO_2/rGO-AM	664.54	3.00	0.6955	2.67	3.48	0.5405

References

[1] A. Rashid, H.N. Bhatti, M. Iqbal, S. Noreen, Fungal biomass composite with bentonite efficiency for nickel and zinc adsorption: A mechanistic study, Ecol. Eng., 91 (2016) 459–471.

[2] M. Mushtaq, H.N. Bhatti, M. Iqbal, S. Noreen, Eriobotrya japonica seed biocomposite efficiency for copper adsorption: Isotherms, kinetics, thermodynamic and desorption studies, J. Environ. Manage., 176 (2016) 21–33.

[3] A. Ehsan, H.N. Bhatti, M. Iqbal, S. Noreen, Native, acidic pretreated and composite clay efficiency for the adsorption of dicationic dye in aqueous medium, Water Sci. Tech., 75 (2017) 753–764.

[4] Z. Ji, X. Shen, M. Li, H. Zhou, G. Zhu, K. Chen, Synthesis of reduced graphene oxide/CeO_2 nanocomposites and their photocatalytic properties, Nanotechnology, 24 (2013) 1–9.

[5] A.R. Contreras, A. García, E. González, E. Casals, V. Puntes, A. Sánchez, X. Font, S. Recillas, Potential use of CeO_2, TiO_2 and Fe_3O_4 nanoparticles for the removal of cadmium from water, Desal. Water Treat., 41 (2012) 296–300.

[6] S. Recillas, A. García, E. González, E. Casals, V. Puntes, A. Sánchez, X. Font, Use of CeO_2, TiO_2 and Fe_3O_4 nanoparticles for the removal of lead from water. Toxicity of nanoparticles and derived compounds, Desalination, 277 (2011) 213–220.

[7] S. Recillas, J. Colón, E. Casals, E. González, V. Puntes, A. Sánchez, X. Font, Chromium (VI) adsorption on cerium oxide nanoparticles and morphology changes during the process, J. Hazard. Mater., 184 (2010) 425–431.

[8] S. Wu, K. Zhang, X. Wang, Y. Jia, B. Sun, T. Luo, F. Meng, Z. Jin, D. Lin, W. Shen, L. Kong, J. Liu, Enhanced adsorption of cadmium ions by 3D sulfonated reduced graphene oxide, Chem. Eng. J, 262 (2015) 1292–1302.

[9] S. Wang, H. Sun, H.M.M. Ang, M.O.O. Tadé, Adsorptive remediation of environmental pollutants using novel graphene-based nanomaterials, Chem. Eng. J., 226 (2013) 336–347.

[10] K. Lü, G.X. Zhao, X.K. Wang, A brief review of graphene-based material synthesis and its application in environmental pollution management, Chinese Sci. Bull., 57 (2012) 1223–1234.

[11] R.L. White, C.M. White, H. Turgut, A. Massoud, Z.R. Tian, Comparative studies on copper adsorption by graphene oxide and functionalized graphene oxide nanoparticles, J. Taiwan Inst. Chem. Eng., 85 (2018) 18–28.

[12] Y. Wen, H. Ding, Y. Shan, Preparation and visible light photocatalytic activity of Ag/TiO_2/graphene nanocomposite, Nanoscale, 3 (2011) 4411–4417.

[13] K. Singh, A. Ohlan, V.H. Pham, B. R, S. Varshney, J. Jang, S.H. Hur, W.M. Choi, M. Kumar, S.K. Dhawan, B.S. Kongd, J.S. Chung, Nanostructured graphene/Fe_3O_4 incorporated polyaniline as a high performance shield against electromagnetic pollution, Nanoscale, 5 (2013) 2411–2420.

[14] A.E. Burakov, E.V. Galunin, I.V. Burakova, A.E. Kucherova, S. Agarwal, A.G. Tkachev, V.K. Gupta, Adsorption of heavy metals on conventional and nanostructured materials for wastewater treatment purposes: A review, Ecotoxicol. Environ. Saf., 148 (2018) 702–712.

[15] T.S. Sreeprasad, S.M. Maliyekkal, K.P. Lisha, T. Pradeep, Reduced graphene oxide-metal/metal oxide composites: facile synthesis and application in water purification, J. Hazard. Mater., 186 (2011) 921–931.

[16] H. Wang, X. Yuan, Y. Wu, H. Huang, X. Peng, G. Zeng, H. Zhong, J. Liang, M. Ren, Graphene-based materials: fabrication, characterization and application for the decontamination of wastewater and waste gas and hydrogen storage/generation, Adv. Colloid Interface Sci., 195–196 (2013) 19–40.

[17] K.C. Kemp, H. Seema, M. Saleh, N.H. Le, K. Mahesh, V. Chandra, K.S. Kim, Environmental applications using graphene composites: water remediation and gas adsorption, Nanoscale, 5 (2013) 3149–3171.

[18] F. Zhang, Ceria nanoparticles: Size, size distribution, and shape, J. Appl. Phys., 95 (2004) 4319–4326.

[19] Q. Ling, M. Yang, R. Rao, H. Yang, Q. Zhang, H. Liu, A. Zhang, Simple synthesis of layered CeO_2–graphene hybrid and their superior catalytic performance in dehydrogenation of ethylbenzene, Appl. Surf. Sci., 274 (2013) 131–137.

[20] R. Sitko, B. Zawisza, E. Malicka, Graphene as a new sorbent in analytical chemistry, TrAC Trends Anal. Chem., 51 (2013) 33–43.

[21] T. Yu, J. Zeng, B. Lim, Y. Xia, Aqueous-phase synthesis of Pt/CeO_2 hybrid nanostructures and their catalytic properties, Adv. Mater., 22 (2010) 5188–5192.

[22] J.W.S. Hummers, R.E. Offeman, Preparation of Graphitic Oxide, J. Am. Chem. Soc., 80 (1958) 1339.
[23] H.K. Boparai, M. Joseph, D.M. O'Carroll, Kinetics and thermodynamics of cadmium ion removal by adsorption onto nano zerovalent iron particles, J. Hazard. Mater., 186 (2011) 458–465.
[24] J.-G. Yu, L.-Y. Yu, H. Yang, Q. Liu, X.-H. Chen, X.-Y. Jiang, X.-Q. Chen, F.-P. Jiao, Graphene nanosheets as novel adsorbents in adsorption, preconcentration and removal of gases, organic compounds and metal ions, Sci. Total Environ., 502 (2015) 70–79.
[25] A.R. Contreras Rodríguez, A. Sánchez, X. Font, Removal of cadmium (II), lead (II) and chromium (VI) in water with nanomaterials, PhD Thesis, Universitat Autònoma de Barcelona, 2015.
[26] F. Zhang, S.-W.W. Chan, J.E. Spanier, E. Apak, Q. Jin, R.D. Robinson, I.P. Herman, Cerium oxide nanoparticles: Size-selective formation and structure analysis, Appl. Phys. Lett., 80 (2002) 127–129.
[27] B. Sabu, T. Varghese, Structural characterization and optical studies of CeO_2 nanoparticles synthesized by chemical precipitation, Indian J. Pure Appl. Phys., 53 (2015) 596–603.
[28] Y. Hernandez, V. Nicolosi, M. Lotya, F.M. Blighe, Z. Sun, S. De, I.T. McGovern, B. Holland, M. Byrne, Y.K. Gun'Ko, J.J. Boland, P. Niraj, G. Duesberg, S. Krishnamurthy, R. Goodhue, J. Hutchison, V. Scardaci, A.C. Ferrari, J.N. Coleman, High-yield production of graphene by liquid-phase exfoliation of graphite, Nat. Nanotechnol., 3 (2008) 563–568.
[29] S. Qaiser, A.R. Saleemi, M. Umar, Biosorption of lead from aqueous solution by Ficus religiosa leaves: batch and column study, J. Hazard. Mater., 166 (2009) 998–1005.
[30] Y. Zhang, C. Banks, A comparison of the properties of polyurethane immobilised Sphagnum moss, seaweed, sunflower waste and maize for the biosorption of Cu, Pb, Zn and Ni in continuous flow packed columns., Water Res., 40 (2006) 788–798.
[31] V.K. Gupta, I. Ali, Removal of lead and chromium from wastewater using bagasse fly ash-a sugar industry waste, J. Colloid Interface Sci., 271 (2004) 321–328.
[32] M. Sánchez-Polo, J. Rivera-Utrilla, Adsorbent-adsorbate interactions in the adsorption of Cd(II) and Hg(II) on ozonized activated carbons, Environ. Sci. Technol., 36 (2002) 3850–3854.
[33] J. Goel, K. Kadirvelu, C. Rajagopal, V.K. Garg, Cadmium (II) uptake from aqueous solution by adsorption on carbon aerogel using a response surface methodological approach, Ind. Eng. Chem. Res., 45 (2006) 6531–6537.
[34] R. Balasubramanian, S.V. Perumal, K. Vijayaraghavan, Equilibrium isotherm studies for the multicomponent adsorption of lead, zinc and cadmium onto Indonesian peat, Ind. Eng. Chem. Res., 48 (2009) 2093–2099.
[35] R. Sitko, E. Turek, B. Zawisza, E. Malicka, E. Talik, J. Heimann, A. Gagor, B. Feist, R. Wrzalik, Adsorption of divalent metal ions from aqueous solutions using graphene oxide, Dalton Trans., 42 (2013) 5682–5689.
[36] G. Zhao, J. Li, X. Ren, C. Chen, X. Wang, Few-layered graphene oxide nanosheets for heavy metal ion pollution management, Environ. Sci. Technol., 45 (2011) 1–4.
[37] Patiha, E. Heraldy, Y. Hidayat, M. Firdaus, The langmuir isotherm adsorption equation: The monolayer approach, IOP Conf. Ser.: Mater. Sci. Eng., 107 (2016) 012067.
[38] J. Wang, B. Chen, Adsorption and coadsorption of organic pollutants and a heavy metal by graphene oxide and reduced graphene materials, Chem. Eng. J., 281 (2015) 379–388.
[39] Y. Sun, Q. Wang, C. Chen, X. Tan, X. Wang, Interaction between Eu(III) and graphene oxide nanosheets investigated by batch and extended X-ray absorption fine structure spectroscopy and by modeling techniques, Environ. Sci. Technol., 46 (2012) 6020–6027.
[40] G. Zhao, T. Wen, X. Yang, S. Yang, J. Liao, J. Hu, D. Xiao, X. Wang, Preconcentration of U(vi) ions on few-layered graphene oxide nanosheets from aqueous solutions, Dalt. Trans., 41 (2012) 6182–6188.
[41] C.Y. Cao, Z.M. Cui, C.Q. Chen, W.G. Song, W. Cai, Ceria hollow nanospheres produced by a template-free microwave-assisted hydrothermal method for heavy metal ion removal and catalysis, J. Phys. Chem. C, 114 (2010) 9865–9870.
[42] K.Y. Foo, B.H. Hameed, Insights into the modeling of adsorption isotherm systems, Chem. Eng. J., 156 (2010) 2–10.
[43] B.H. Hameed, I.A.W. Tan, A.L. Ahmad, Adsorption isotherm, kinetic modeling and mechanism of 2,4,6-trichlorophenol on coconut husk-based activated carbon, Chem. Eng. J., 144 (2008) 235–244.
[44] G. Alagumuthu, V. Veeraputhiran, R. Venkataraman, Adsorption isotherms on fluoride removal: Batch Techniques, Arch. Appl. Sci. Res., 2 (2010) 170–185.
[45] V. Chandra, J. Park, Y. Chun, J.W. Lee, I.C. Hwang, K.S. Kim, Water-dispersible magnetite-reduced graphene oxide composites for arsenic removal, ACS Nano., 4 (2010) 3979–3986.

Supplementary Information

SI.1. Instrumental parameters for ICP-OES analysis.

Table S1
Instrumental parameters for ICP-OES analysis

Instrumental parameters	
Premix chamber	Scott
Nebulizer	Cross-flow
Injector	Alumina 2 mm ID
Gas flow	Plasma (15 L/min)
	Auxiliary (0.2 L/min)
Overview	Nebulizer (0.75 L/min)
Axial	RF power (13000 W)
	Pump (1.5 ml/min)

SI.2. Nanoparticles size distribution. Histogram parameters

The NPs size distribution parameters of the three synthetized samples. Diameters were measured with the Image J software program and the average values were calculated by counting a minimum of 100 particles.

Table S2
Histogram parameters of the measured nanoparticles with the Image J software counting a minimum of 100 particles

CeO_2/rGo-HMT						
	Area	Mean	Min	Max	Angle	Length
Mean	0.397	99.924	70.356	134.902	–42.922	3.343
SD	0.125	23.381	24.179	27.771	59.967	0.701
Min	0.202	46.673	25.333	76.603	–135	1.856
Max	0.767	140.226	118.089	188.667	137.726	5.489

CeO_2/rGo-AHA						
	Area	Mean	Min	Max	Angle	Length
Mean	2.382	92.161	62.353	137.171	–16.172	16.121
SD	0.911	26.171	25.892	31.18	55.974	2.245
Min	0.679	33.297	0.667	57.168	–144.819	10.922
Max	4.282	150.411	120.576	223.798	128.395	23.341

CeO_2/rGo-AM						
	Area	Mean	Min	Max	Angle	Length
Mean	0.152	73.569	44.289	108.528	–17.878	2.106
SD	0.046	19.715	19.756	24.664	53.329	0.399
Min	0.079	33.367	7.143	47	–137.121	1.367
Max	0.244	114.265	88.62	152	65.376	3.102